Elucidating the structural basis of diphenyl ether derivatives as highly potent enoyl-ACP reductase inhibitors through molecular dynamics simulations and 3D-QSAR study

6 AUTHORS, INCLUDING:

Pharit Kamsri
Ubon Ratchathani University
9 PUBLICATIONS **4** CITATIONS

SEE PROFILE

Auradee Punkvang
Nakhonphanom University
14 PUBLICATIONS **46** CITATIONS

SEE PROFILE

Supa Hannongbua
Kasetsart University
175 PUBLICATIONS **1,345** CITATIONS

SEE PROFILE

Stephan Irle
Nagoya University
202 PUBLICATIONS **3,177** CITATIONS

SEE PROFILE

Elucidating the structural basis of diphenyl ether derivatives as highly potent enoyl-ACP reductase inhibitors through molecular dynamics simulations and 3D-QSAR study

Pharit Kamsri · Auradee Punkvang · Patchareenart Saparpakorn · Supa Hannongbua · Stephan Irle · Pornpan Pungpo

Abstract Diphenyl ether derivatives are good candidates for anti-tuberculosis agents that display a promising potency for inhibition of InhA, an essential enoyl-acyl carrier protein (ACP) reductase involved in fatty acid biosynthesis pathways in *Mycobacterium tuberculosis*. In this work, key structural features for the inhibition were identified by 3D-QSAR CoMSIA models, constructed based on available experimental binding properties of diphenyl ether inhibitors, and a set of four representative compounds was subjected to MD simulations of inhibitor-InhA complexes for the calculation of binding free energies. The results show that bulky groups are required for the R_1 substituent on the phenyl A ring of the inhibitors to favor a hydrophobic pocket formed by residues Phe149, Met155, Pro156, Ala157, Tyr158, Pro193, Met199, Val203, Leu207, Ile215, and Leu218. Small substituents with a hydrophilic property are required at the R_3 and R_4 positions of the inhibitor phenyl B rings to form hydrogen bonds with the backbones of Gly96 and Met98, respectively. For the R_2 substituent, small substituents with simultaneous hydrophilic or hydrophobic properties are required to favor the interaction with the pyrophosphate moiety of NAD^+ and the methyl side chain of Ala198, respectively. The reported data provide structural guidance for the design of new and potent diphenyl ether-based inhibitors with high inhibitory activities against *M. tuberculosis* InhA.

P. Kamsri · P. Pungpo (✉)
Department of Chemistry, Faculty of Science, Ubon Ratchathani University, 85 Sthollmark Rd., Warinchamrap, Ubonratchathani 34190, Thailand
e-mail: pornpan_ubu@yahoo.com

A. Punkvang
Faculty of Liberal Arts and Sciences, Division of Science, Nakhon Phanom University, Nakhon Phanom 48000, Thailand

P. Saparpakorn · S. Hannongbua
Department of Chemistry, Faculty of Science, Kasetsart University, Chatuchak, Bangkok 10900, Thailand

S. Irle
Institute of Transformative Bio-Molecules (WPI-ITbM) and Department of Chemistry, Graduate School of Science, Nagoya University, Furo-cho, Chikusa-ku, Nagoya 464-8602, Japan

Introduction

Tuberculosis (TB), caused by pathogenic bacterial species *Mycobacterium tuberculosis*, remains a major global health problem and ranks as the second-leading cause of death from an infectious disease worldwide, after the human immunodeficiency virus (HIV). The latest estimates included in World Health Organization (WHO) report were 8.6 million new TB cases and 1.3 million TB deaths in 2012 [1]. The enoyl-acyl carrier protein (ACP) reductase (InhA) catalyzes the NADH-specific reduction of α,β-unsaturated fatty acids bound to the enoyl-ACP, the last step of fatty acids biosynthesis in *M. tuberculosis* [2, 3], and is an attractive target to design novel antitubercular drugs [4–10]. Moreover, InhA has been identified as the primary target of the most effective first-line anti-TB drug, isoniazid (INH) [11–19]. INH is a prodrug that is activated by catalase-peroxidase (KatG) enzymes to form an acyl radical that binds covalently to nicotinamide adenine dinucleotide (NAD^+) at the position 4, producing an active INH-NAD adduct [20–25] that functions as a highly potent inhibitor of InhA [26, 27]. However, such high potency of

INH for tuberculosis treatment can be diminished if mutations arise in KatG, as found in previous clinical studies [18, 28]. Therefore, new inhibitors targeting the InhA without the activation process from KatG are required. The first inhibitor, triclosan, inhibiting the InhA directly has been reported [29]. Based on the mechanism action of triclosan, triclosan and diphenyl ether derivatives have been developed by using structure-based drug design [30–35]. A diphenyl ether derivative, 5-octyl-2-phenoxy phenol, shows the highest potent InhA inhibitor with IC_{50} of 5 nM [33]. Recently, molecular modeling and computer-aided molecular design approaches have been performed to develop the InhA inhibitors [36–48]. To gain insight into the structural requirement of highly potent diphenyl ether derivatives as the InhA inhibitors, three-dimensional quantitative structure–activity relationships (3D-QSAR) based on comparative molecular similarity indices analysis (CoMSIA) was performed. Moreover, molecular dynamics (MD) simulations were also performed to gain deeper insight into a fundamental basis of structural behavior, inhibitor–InhA interactions and thermodynamic properties. The molecular information obtained from both CoMSIA and MD simulations should be valuable for the design of new and better InhA inhibitors as anti-tubercular agents.

Materials and methods

Data sets for QSAR study

The 52 diphenyl ether derivatives [30, 31, 33, 35] listed in Table 1 were used to build the CoMSIA model. The experimentally obtained IC_{50} values of each compound for InhA inhibition were converted to the corresponding log $(1/IC_{50})$ values and used as dependent variables for the QSAR model. The chemical structures of these compounds were constructed using standard tools available in the GaussView 3.07 program [49] and were then fully optimized using the ab initio quantum chemical method (HF/3-21G) implemented in the Gaussian 09 program [50]. The compounds were divided into a training set of 43 compounds, and a test set of nine compounds for model development and validation, respectively. The test set was randomly selected based on a structural diversity and wide range of activity in the data sets.

Molecular docking calculations

The X-ray crystal structure of diphenyl ether complexed with InhA (PDB code 2X23) [34] was used as a template for molecular docking calculations. Docking calculations for all 52 diphenyl ether derivatives were carried out by the Autodock 4.02 program using the Lamarckian genetic algorithm (LGA) [51]. Docking parameters were used as default values, except for the number of docking runs, which was set to 50. The parameters of the docking calculations were validated by successfully reproducing the X-ray conformation of the ligand in the PDB structure 2X23, as well as its orientation in the binding pocket. The RMSD value between original and docked coordinates was lower than 1 Å and therefore acceptable. For all 52 candidate compounds, the ligand pose with the lowest final docked energy was selected as the best binding mode of these potential InhA inhibitors.

CoMSIA study

The binding mode of compound **21**, representing the best active compound for the InhA inhibition, was taken from the X-ray structure (PDB code 2B37) [33] and used as a template for molecular alignment. The pharmacophore alignment module with the GALAHAD fit implemented in SYBYL 8.0 program [52] was employed to align all compounds to the molecular template. SYBYL 8.0 molecular modeling software was then used to construct CoMSIA models. Five CoMSIA descriptors including steric, electrostatic, hydrophobic, hydrogen bond donor, and hydrogen bond acceptor fields were calculated using an sp^3 carbon probe atom, with a formal charge of +1, which was placed at the intersections in a grid spacing of 2 Å. CoMSIA descriptors were set as independent variables and log $(1/IC_{50})$ values were used as dependent variables in the partial least square (PLS) analysis to derive a linear relationship between molecular descriptors and activities. The cross-validation was performed using the leave-one-out method with a 2.0-kcal/mol^{-1} column filter to minimize the influence of noisy columns. A final non-cross-validated analysis with the optimal number of components was sequentially performed and was then employed to analyze the results. The non-cross-validated correlation coefficient (r^2) and the leave-one-out (LOO) cross-validated correlation coefficient (q^2) were used to evaluate the predictive ability of the CoMSIA model. To estimate the predictive abilities of the best CoMSIA model, external validation using several statistical data was employed. According to Golbraikh and Tropsha [53], the best CoMSIA model is considerably acceptable if they satisfy all of the following criteria: $q^2 > 0.50$, $r^2 > 0.60$, and $0.85 \leq k \leq 1.15$.

MD simulations

In a subsequent step, MD simulations were performed on compounds **17**, **18**, **19**, and **29**, which are representative compounds that cover a wide range from highly active (**17** and **29**) to less active compounds (**18**) among the candidate series in this study. Compound **19** was also included in the simulations to represent a moderate inhibitory activity.

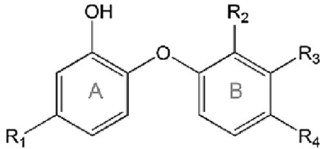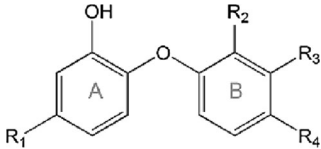**Table 1** The chemical structures and activities for InhA inhibition of 52 diphenyl ether derivatives

Cpd.	R_1	R_2	R_3	R_4	IC_{50}(nM)	Log(1/IC_{50}) Exp.	CoMSIA	Res.
1	Cl	Cl	H	Cl	1,100	5.96	6.03	−0.07
2	CH_3	Cl	H	Cl	800	6.10	6.12	−0.02
3	CH_2Cy	Cl	H	Cl	110	6.96	6.91	0.05
4[a]	CH_2CH_3	Cl	H	Cl	120	6.92	6.80	0.12
5	$(CH_2)_2CH_3$	Cl	H	Cl	91	7.04	6.84	0.20
6	$(CH_2)_3CH_3$	Cl	H	Cl	55	7.26	7.24	0.02
7	$(CH_2)_2CH(CH_3)_2$	Cl	H	Cl	63	7.20	7.27	−0.07
8	$CH_2CH(CH_3)CH_2CH_3$	Cl	H	Cl	130	6.89	6.78	0.11
9	CH_2(2-pyridyl)	Cl	H	Cl	29	7.54	7.39	0.15
10[a]	CH_2(3-pyridyl)	Cl	H	Cl	42	7.38	6.87	0.51
11	CH_2(4-pyridyl)	Cl	H	CN	75	7.12	6.98	0.14
12	o-CH_3-Ph	Cl	H	Cl	1,300	5.89	5.96	−0.07
13	m-CH_3-Ph	Cl	H	Cl	870	6.06	5.96	0.10
14	CH_2Ph	Cl	H	Cl	51	7.29	7.29	0.00
15	CH_2CH_2Ph	Cl	H	Cl	21	7.68	7.81	−0.13
16[a]	$(CH_2)_3Ph$	Cl	H	Cl	50	7.30	6.89	0.41
17	$(CH_2)_5CH3$	H	H	H	11	7.96	7.38	0.58
18	CH_2CH_3	H	H	H	2,000	5.70	6.33	−0.63
19	$(CH_2)_3CH_3$	H	H	H	80	7.10	7.47	−0.37
20	$(CH_2)_4CH_3$	H	H	H	17	7.77	7.78	−0.01
21	$(CH_2)_7CH_3$	H	H	H	5	8.30	8.23	0.08
22	$(CH_2)_{13}CH_3$	H	H	H	150	6.82	7.31	−0.49
23[a]	$(CH_2)_5CH_3$	NO_2	H	H	180	6.74	6.73	0.01
24	$(CH_2)_5CH_3$	H	NO_2	H	48	7.32	7.38	−0.05
25	$(CH_2)_5CH_3$	H	H	NO_2	90	7.05	6.99	0.06
26[a]	$(CH_2)_5CH_3$	NH_2	H	H	62	7.21	6.93	0.28
27	$(CH_2)_5CH_3$	H	NH_2	H	1,090	5.96	5.94	0.02
28	$(CH_2)_5CH_3$	H	H	NH_2	55	7.26	7.27	−0.01
29	$(CH_2)_5CH_3$	Br	H	H	10	8.00	7.93	0.07
30[a]	$(CH_2)_5CH_3$	CF_3	H	H	29.7	7.53	7.36	0.17
31	$(CH_2)_5CH_3$	F	H	H	12.1	7.92	7.92	0.00
32	$(CH_2)_5CH_3$	I	H	H	44.6	7.35	7.39	−0.04
33	$(CH_2)_5CH_3$	OH	H	H	48	7.32	7.29	0.03
34	$(CH_2)_5CH_3$	CN	H	H	235.6	6.63	6.72	−0.09
35	$(CH_2)_5CH_3$	Cl	H	H	49.5	7.31	7.51	−0.20
36[a]	$(CH_2)_5CH_3$	CH_3	H	H	50.7	7.29	7.14	0.15
37	$(CH_2)_5CH_3$	$NHCOCH_3$	H	H	1,550	5.81	5.88	−0.07
38	$(CH_2)_5CH_3$	H	H	$NHCONH_3$	1,300	5.89	5.87	0.02
39	$(CH_2)_5CH_3$	$NHCOCO_2H$	H	H	2,360	5.63	5.72	−0.09
40	$(CH_2)_5CH_3$	H	$NHCOCO_2H$	H	580	6.24	6.32	−0.08
41	$(CH_2)_5CH_3$	H	H		1,930	5.71	5.62	0.09
42[a]	$(CH_2)_5CH_3$	H	NHCO- isoxazole	H	1,220	5.91	6.08	−0.17

Table 1 (continued)

Cpd.	R_1	R_2	R_3	R_4	IC_{50}(nM)	Log(1/IC_{50})		
						Exp.	CoMSIA	Res.
43	$(CH_2)_5CH_3$	CH_2-N-CH_3-piperazine	H	H	1,315	5.88	5.76	0.12
44	$(CH_2)_5CH_3$	H	H	CH_2-N-CH_3-piperazine	306	6.51	6.53	−0.02
45	CH_2CH_2Ph	H	H	H	144.3	6.84	6.89	−0.05
46	CH_2CH_2Ph	CH_3	H	H	360.1	6.44	6.33	0.12
47	CH_2Ph	Cl	H	H	20.08	7.70	7.44	0.26
48	CH_2Ph	H	H	H	49.6	7.30	7.27	0.03
49	CH_2Ph	CH_3	H	H	56.4	7.25	7.59	−0.34
50	$CH_2CH_2CH_2OH$	CH_3	H	H	4,326	5.36	5.25	0.11
51	$OCH_2CH_2OCH_3$	H	H	H	253.1	6.60	6.55	0.05
52[a]	$O(CH_2)_4CH_3$	H	H	H	94.2	7.03	7.32	−0.29

[a] Test set

Complex InhA structures of these compounds as generated by the previous docking calculations were used as initial coordinates for MD simulations. The AMBER12 [54] software suite was used for all MD simulations to classically describe all relevant interactions within the system: InhA protein was described by the *ff03* force field [55] while NAD^+ and diphenyl ether inhibitors were described by the general AMBER force field (GAFF) [56, 57]. All missing hydrogen atoms of InhA were added using the LEaP module. To obtain the partial atomic charges of diphenyl ether derivatives and NAD^+, the geometry optimization and electrostatic potential calculation of each compound was first calculated at the HF/6-31G* level using the Gaussian 09 program [50]. Then, RESP partial charges [58–62] were assigned using the ANTECHAMBER module implemented in AMBER12. Each complex structure was solvated by TIP3P [63] waters in a truncated octahedral box extending up to 10 Å from each solute species. Five Na^+ cations were added to neutralize the charge in each system. Non-bonded cut-off was set to 10 Å. To relieve bad steric interactions that originated from addition of the water molecules and ions, the systems were first minimized with atomic positions of all solute species restraint (using a force constant of 500 kcal/mol^{-1} $Å^2$). Then, the whole system was fully minimized without restraining conditions. The solvated systems were gradually warmed up from 0 to 300 K in the first 20 ps followed by maintaining the temperature at 300 K during the last 10 ps. An integration time-step of 2 fs was used in a constant volume boundary. After minimization and heating, the position-restrained dynamics

simulations were performed for 70 ps at 300 K under an isobaric condition to relax the positions of the solvent molecules. A weak force constant of 10 kcal/mol^{-1} $Å^2$ restraint on solute species was also applied for each simulation. Then, a 5-ns production MD simulation without restraints was performed on each system at a constant temperature of 300 K under isobaric condition. The Particle Mesh Ewald (PME) [64] was applied to treat the long-range electrostatic interactions with a periodic boundary condition during the MD simulations. The cut-off distance for the long-range van der Waals interaction was set to 8 Å. The SHAKE [65] method was applied to constrain the bond lengths of hydrogen atoms attached to heteroatoms. Coordinates and energy outputs during the MD simulation were collected every 2 ps. Finally, the root-mean-square deviations (RMSDs) of the InhA protein, NAD^+, and diphenyl ether ligand, respectively, were analyzed along the MD trajectory relative to the initial structures to determine the stability of the system. The binding free energies were calculated to evaluate the binding affinities of diphenyl ether derivatives in the InhA binding pocket.

Binding free energy calculation

The free energy of binding between InhA and diphenyl ether inhibitors were calculated using the Molecular Mechanics Poisson–Boltzmann Surface Area (MM-PBSA) [66–69] and Normal-mode [70] methods. For MM-PBSA calculation, 125 snapshots were generated

for each complex from the last 1 ns of MD trajectory with an interval of 8 ps. The binding free energies (ΔG_{bind}) were obtained using Eqs. (1–4).

$$\Delta G_{bind} = G_{com} - (G_{rec} + G_{ligand}) \qquad (1)$$

$$\Delta G_{bind} = \Delta H - T\Delta S \qquad (2)$$

$$\Delta H = \Delta G_{MM} + \Delta G_{solv} \qquad (3)$$

$$\Delta G_{bind} = \Delta G_{MM} + \Delta G_{sol} - T\Delta S \qquad (4)$$

where G_{com}, G_{rec}, and G_{ligand} are the free energies of the complex, InhA and the diphenyl ether inhibitors, respectively. In general, the binding free energy is composed of an enthalpic (ΔH) and an entropic contribution ($T\Delta S$). The enthalpic contribution (ΔH) contains the gas-phase molecular mechanics energy (ΔG_{MM}) and the solvation free energy (ΔG_{solv}) as shown in Eq. (3). The entropic contribution ($T\Delta S$) to the binding free energy was estimated using normal-mode analysis with AMBER Nmode module. Due to a highly computational cost in the entropy calculation, the residues around the ligand (less than 12 Å) were only considered

as the receptor for normal-mode calculations [69, 71]. For this calculation, 50 snapshots were extracted from the last 1 ns of MD trajectory with an interval of 20 ps.

Results and discussion

MD simulation

System equilibration

Four MD simulations of compounds **17**, **18**, **19**, and **29** bound with InhA were performed for 5 ns to evaluate the structural stability of the complexes and their binding strength. The RMSDs for all atoms of three different solute species (InhA, NAD$^+$, and inhibitor) relative to the initial structure over the 5 ns of simulation times were analyzed and plotted in Fig. 1. The plateau characteristic of the RMSD plot over the simulation time is the criteria to indicate the equilibrium state of each solute species. Figure 1 shows that NAD$^+$ and compounds **17**, **18**, **19**, and **29** reach the equilibrium state at the early time. However, RMSDs of all compounds are more fluctuated, particularly compound **17**. InhA complexed with compounds **17**, **18**, **19**, and **29** reach the equilibrium state after 1.0 ns (Fig. 1a), 1.5 ns (Fig. 1b), 2.5 ns (Fig. 1c), and 1.0 ns (Fig. 1d), respectively. Moreover, to reveal the energy stability of each system, the receptor–ligand interaction energies of
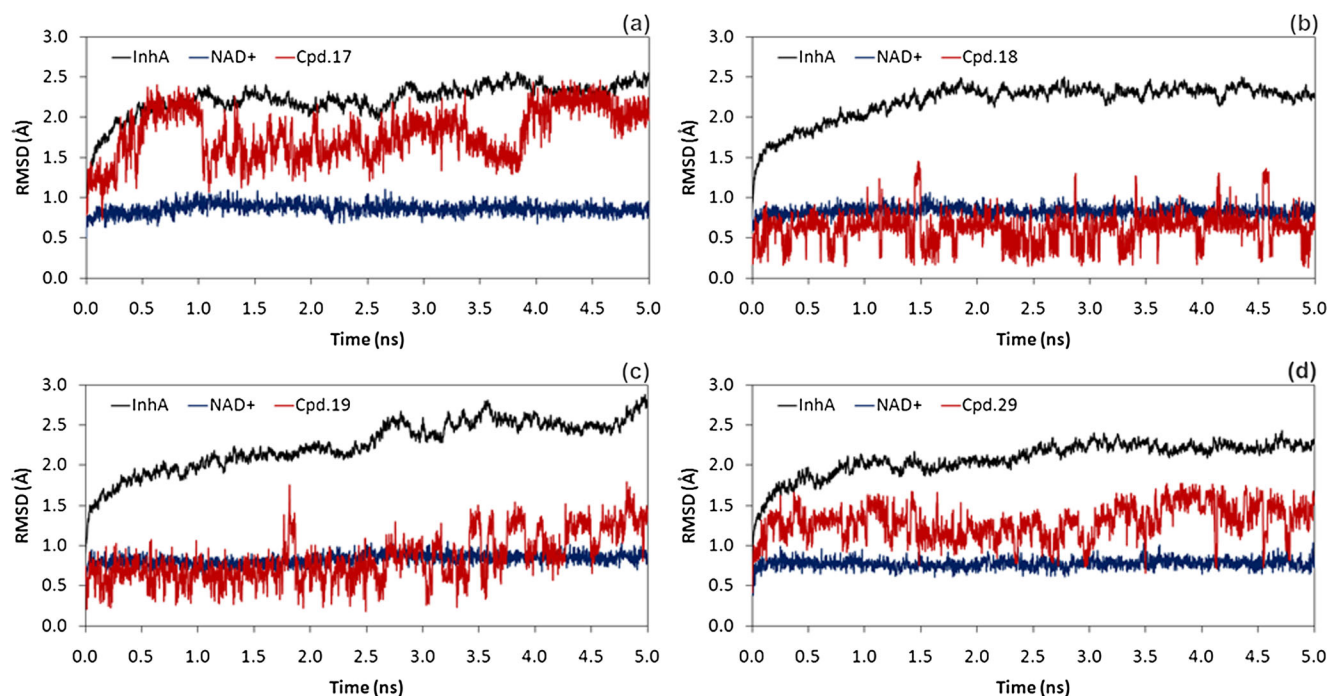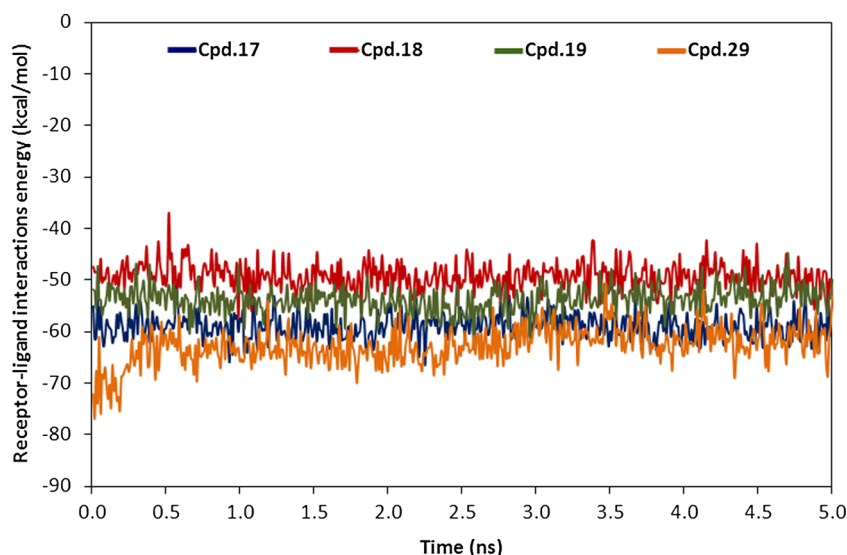

Fig. 1 RMSD plots of compounds **17** (**a**), **18** (**b**), **19** (**c**), and **29** (**d**) complexed with InhA

Fig. 2 Receptor–ligand interaction energies for the systems of compounds **17** (**a**), **18** (**b**), **19** (**c**), and **29** (**d**) over the 5 ns simulation

compounds **17**, **18**, **19**, and **29** over the 5-ns simulation time were calculated by MM-PBSA method. The receptor–ligand interaction energies of all compounds reach the equilibrium state at the beginning of the simulation time, except that of compound **29**, which reaches the equilibrium state after the 0.5 ns simulation time (Fig. 2). The average receptor–ligand interaction energies of compounds **17**, **18**, **19**, and **29** are -58.85 ± 2.42, -49.27 ± 2.55, -53.85 ± 2.46, and -62.72 ± 3.55 kcal/mol^{-1}, respectively. Based on the receptor–ligand interaction energy and RMSD plots, Compounds **17**, **18**, **19** and **29** complexed with InhA are sufficiently stable and the production simulations are reliable. Therefore, the subsequent free energy calculation and free energy decomposition analysis based on snapshots extracted from the stable state are reasonable.

Binding free energy calculations

The MM-PBSA method was employed to calculate the binding free energies of compounds **17**, **18**, **19**, and **29** in InhA and

the results are shown in Table 2. The binding free energies (ΔG_{bind}) of compounds **17**, **18**, **19**, and **29** bound to the InhA pocket are calculated to be -15.02, -9.03, -13.90, and -15.40 kcal/mol^{-1}, respectively, which are in good agreement with those determined experimentally ($\Delta G_{exp.}$). Pearson correlation and Spearman rank correlation [72] were employed to determine the correlation between $\Delta G_{exp.}$ and ΔG_{bind}. The accepted values of correlation coefficient are in the range of -1 to 1. Based on these methods, the correlation between $\Delta G_{exp.}$ and ΔG_{bind} shows the correlation coefficient of Pearson correlation and Spearman rank correlation to be 0.98 and 1.00, respectively. Therefore, there is the correlation between $\Delta G_{exp.}$ and ΔG_{bind}.

The binding modes of diphenyl ether derivatives in InhA

The binding modes of compounds **17**, **18**, **19**, and **29** bound with InhA pocket observed from the simulations are superimposed and illustrated in Fig. 3. In general, all compounds showed a similar binding mode and conformation: the OH group of the phenyl A ring lies in between the OH groups of Tyr158 and ribose fragment of NAD$^+$ to form the hydrogen bond interactions. The phenyl A ring forms the pi–pi interaction with pyridine amide ring of NAD$^+$. As the phenyl A ring bearing the R_1 substituent as the alkyl chain, it is placed in the hydrophobic pocket that is formed by Phe149, Met155, Pro156, Ala157, Tyr158, Pro193, Met199, Val203, Leu207, Ile215, and Leu218 (Fig. 3). Compounds **17** and **29** that hold the hexyl substituents at the R_1 position could form stronger hydrophobic interactions with Phe149, Met155, Pro156, Ala157, Tyr158, Pro193, Met199, Val203, Leu207, Ile215, and Leu218 when comparing these interactions with compounds **18** and **19** that have shorter alkyl substituents (containing ethyl and butyl, respectively), losing several hydrophobic interactions with Pro156, Ala157, Val203, Leu207,

Table 2 The binding free energies (kcal/mol^{-1}) calculated by the MM-PBSA method

| Component	Diphenyl ether-InhA complexes			
	17	18	19	29
ΔG_{MM}	-58.77 ± 2.59	-49.49 ± 2.29	-52.90 ± 2.57	-60.82 ± 2.91
$\Delta G_{solv.}$	21.59 ± 2.07	19.33 ± 1.23	20.13 ± 1.60	22.70 ± 2.69
ΔH	-37.18 ± 2.93	-30.16 ± 2.24	-32.77 ± 2.47	-38.06 ± 3.21
$-T\Delta S$	22.16 ± 0.85	21.13 ± 1.17	18.87 ± 1.06	22.66 ± 0.57
$\Delta G_{bind.}$	-15.02 ± 1.32	$-9.03\pm.084$	-13.90 ± 1.31	-15.40 ± 1.40
$\Delta G_{exp.}$ [a]	-10.93	-7.83	-9.75	-10.99

[a] Derived from $\Delta G = RT \ln[IC_{50}]$, R represents the gas constant (1.988 cal/mol^{-1} K), T represents the temperature (300 K)

Fig. 3 The superimposition of compounds **17** (stick in *cyan color*), **18** (stick in *yellow color*), **19** (stick in *green color*), and **29** (stick in *pink color*) in the InhA pocket obtained from MD simulation
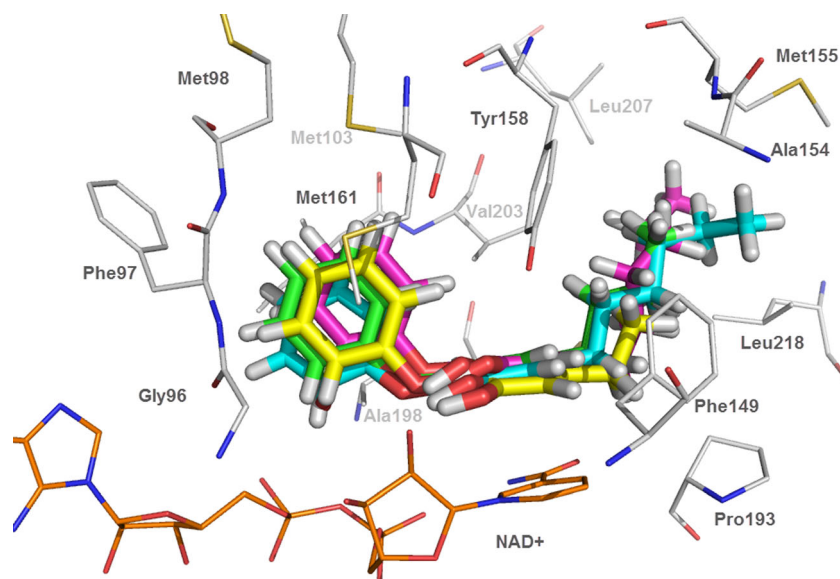
and Ile215. Therefore, the more hydrophobic interactions at the R_1 position of compounds **17** and **29** should account for better activities against InhA. The phenyl B ring containing the R_2, R_3, and R_4 substituents is surrounded by the pyrophosphate moiety of NAD^+, the hydrophilic backbones of Gly96, Met98, Phe97, and the hydrophobic side chains of Met103, Met161, Ile202, Val203, Ala198. The H and Br substituents at the R_2 position for compounds **17** and **29**, respectively, are closed to the methyl side chain of Ala198 and the pyrophosphate moiety of NAD^+ (Fig. 4). The Br substituent of compound **29** contributes greatly a hydrophobic interaction to the methyl side chain of Ala198 while the H substituent of compound **17** contributes a hydrophilic interaction to the ribose and pyrophosphate moieties of NAD^+. These results might explain why compounds **29** and **17** show the InhA inhibitory activities in the same level with IC_{50} of 10 and 11 nM,

respectively. Accordingly, the R_2 substituent would also be hydrophobic or hydrophilic groups. For the R_3 position, the H substituents at this position for compounds **17**, **18**, **19**, and **29** form a hydrogen bond interaction with the carbonyl backbone of Gly96 and, besides the H substituent, other hydrogen bond donor substituents would also be possible. A similar H-bond interaction was also found for the R_4 substituent where all four compounds point to the NH and carbonyl backbone of Met98.

3D-QSAR study

CoMSIA model

The PLS results of CoMSIA models are summarized in Table 3. Ten CoMSIA models were constructed with various combinations of CoMSIA descriptors. Among all models,

Fig. 4 The interactions of the R_2 substituents of compounds **17** and **29** with Ala198 and the pyrophosphate moiety of NAD^+
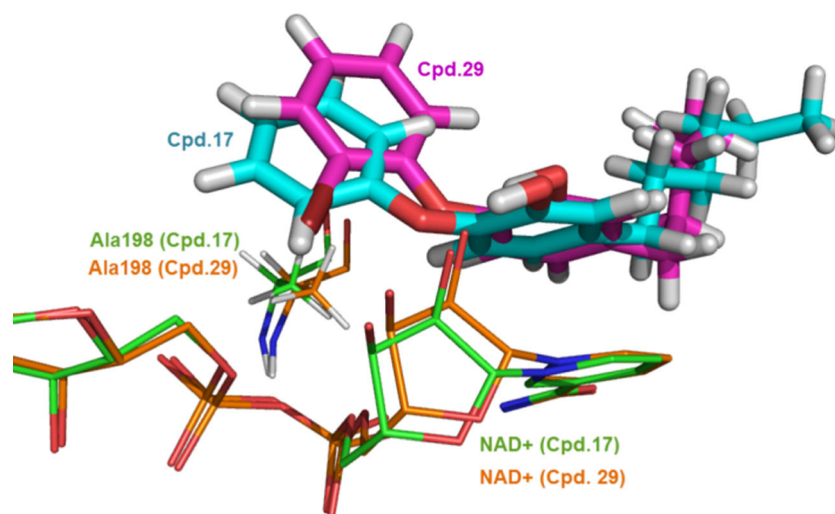
Table 3 Summary of statistical results of CoMSIA models

Models	Statistical data						Fraction
	q^2	r^2	s	SSE	F	N	
1.S/E	0.29	0.93	0.70	0.21	85.48	6	38.6/61.4
2.S/H	0.08	0.69	0.75	0.44	43.53	2	38.8/61.2
3.S/D	0.54	0.89	0.56	0.27	50.30	6	53.7/46.3
4.S/A	0.13	0.88	0.76	0.28	54.86	5	53.5/46.5
5.S/D/E	0.58	0.93	0.54	0.22	77.34	6	27.9/41.7/30.5
6.S/D/H	0.56	0.93	0.55	0.21	85.19	6	29.9/37.6/32.5
7.S/D/A	0.51	0.93	0.58	0.22	76.55	6	39.9/33.1/27.0
8. S/D/E/H	**0.60**	**0.95**	**0.52**	**0.19**	**104.17**	**6**	**19.0/32.5/23.8/24.8**
9. S/D/E/A	0.50	0.93	0.58	0.22	78.66	6	23.9/34.3/25.9/15.9
10.S/D/E/H/A	0.55	0.95	0.55	0.19	103.76	6	17.2/26.6/21.4/22.1/12.8

Bold values indicate the best CoMSIA model

N optimum number of components; *s* standard error of prediction; *SEE* standard error of estimate; *F* F-test value; *S* steric field; *E* electrostatic field; *H* hydrophobic field; *D* hydrogen donor field; *A* hydrogen acceptor field

model 8 composing the steric, hydrogen bond donor, electrostatic and hydrophobic fields is the best CoMSIA model, giving the best statistical parameters with a q^2 value of 0.60 and an r^2 value of 0.95. The predicted activities of 43 compounds in the training set and nine compounds in test set derived from the best CoMSIA model are summarized in Table 1. There is a good correlation between actual and predicted activities of the training set based on the best CoMSIA model, as depicted in Fig. 4. In order to assess the external predictive ability of this model, the InhA inhibitory activities of the test set were predicted. The predicted values of nine test-set compounds are within one logarithmic unit difference from the experimental values (Fig. 5). Therefore, the best CoMSIA model is reliable with highly predictive ability

and could be utilized to predict the InhA activities for newly designed diphenyl ether inhibitors.

The predictive abilities of the best CoMSIA model were determined from the test set including nine compounds. For the best CoMSIA model, internal validation of leave-one-out cross-validated q^2 and predicted r^2 ($r^2_{pred.}$ or r^2) were found to be 0.64 and 0.70, respectively. The calculated square correlation coefficient values between the experimental and predicted values of the test-set compounds with intercept set at zero (r^2_0) and without intercept (r^2) were 0.56 and 0.73, respectively. The slope of regression line through the origin (k) of the best CoMSIA model was 1.02, which is close to 1. Based on the statistical results, the best CoMSIA model could be considered reliable.
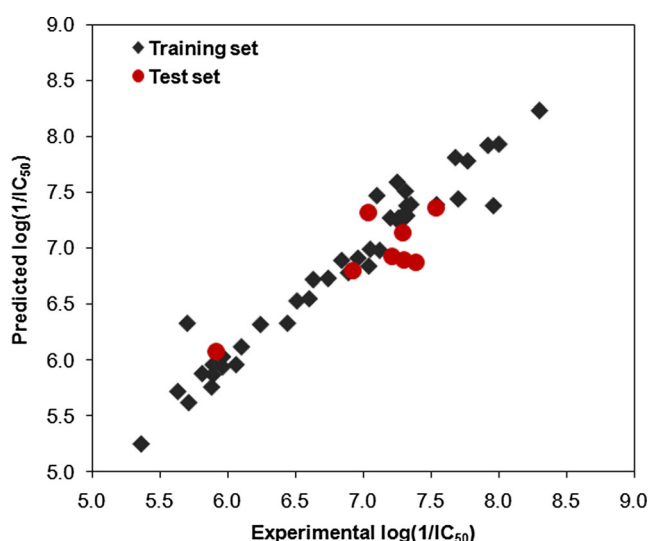
CoMSIA contour maps

To reveal the importance of molecular descriptor fields on InhA inhibitory activities of diphenyl ether derivatives, CoMSIA contour maps were established. Figures 6 and 7 present the CoMSIA contour maps that reveal the influence of steric, electrostatic, hydrophobic, and hydrogen donor fields to the activity of diphenyl ether derivatives. Green and yellow contours indicate areas where favorable and unfavorable steric bulks are predicted to enhance the activities of diphenyl ether derivatives. Blue and red contours indicate regions where electropositive and electronegative groups lead to an increase of the InhA inhibitory activity, respectively. Magenta and white contours represent areas where the hydrophobic group and the hydrophilic group are predicted to favor the biological activities. The cyan and orange contours indicate regions that favor the hydrogen donor group and unfavor hydrogen donor group, respectively. The interpretation of
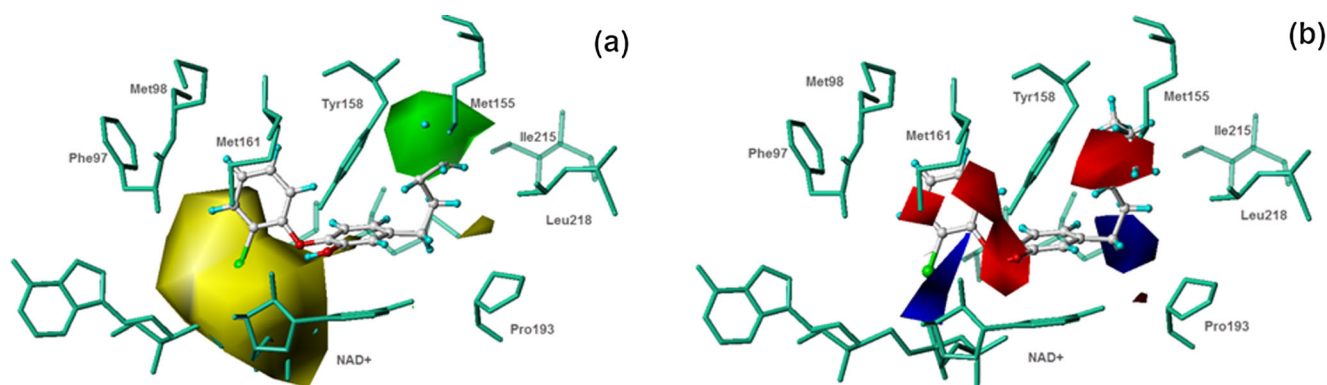

Fig. 5 Plots between the experimental and predicted activities of the training and test sets derived from the CoMSIA model

Fig. 6 CoMSIA steric (**a**) and electrostatic (**b**) contours in combination with compound **29** (ball and stick in atom type colors) in InhA binding pocket (stick in *greenblue*)

CoMSIA contour maps reveals the structural requirement of each substituent position in the scaffold of diphenyl ether derivatives helpful for rational design of novel and potent InhA inhibitors.

Structural requirement for the R₁ positions on the phenyl A ring

The appearance of cyan contours near the OH group of the phenyl A ring emphasizes the important role of this moiety to the InhA inhibitory activity of diphenyl ether derivatives (Fig. 7b). The C4 and C6 atoms of hexyl side chain of compound **29** are covered by green and red contours (Fig. 6a and b). Therefore, the R₁ substituent containing the bulky size and high electron density would be favorable for this region. In case of the R₁ substituent as the alkyl chain, the alkyl chain with the carbon atoms higher than two atoms should be preferable for the InhA inhibitory activity. As exemplified, compound **21**, containing an octyl group at the R₁ position, possesses the most active compound in this series, whereas compound **18** containing ethyl substituent exhibits much lower inhibitory activity than those of compounds **19**,

20, **17**, and **21** bearing butyl, pentyl, hexyl, and octyl substituents at the R₁ position, respectively. Corresponding to the MD results, the longer alkyl chain at R₁ substituent could form hydrophobic interactions more than the shorter alkyl chain.

Structural requirement for the R₂, R₃, and R₄ positions on the phenyl B ring

The unfavorable hydrophobic white contour and the unfavorable steric yellow contour present near the R₂, R₃, and R₄ substituents (Figs. 6a and 7a). These results indicate that the small hydrophilic substituents at the R₂, R₃, and R₄ positions are required for the InhA inhibitory activity of diphenyl ether derivatives. Therefore, compounds **37**–**44** containing the bulky hydrophilic substituents at the R₂, R₃, and R₄ positions show poor activities for InhA inhibition with IC₅₀ more than 360 nM. These suggestions are in agreement with the binding modes of compounds **17**, **18**, **19**, and **29** observed from the MD simulations that the R₂, R₃, and R₄ substituents are located near the pyrophosphate moiety of NAD⁺, the hydrophilic backbones of Gly96 and Met98, respectively. Accordingly, the small substituent with hydrophilic property
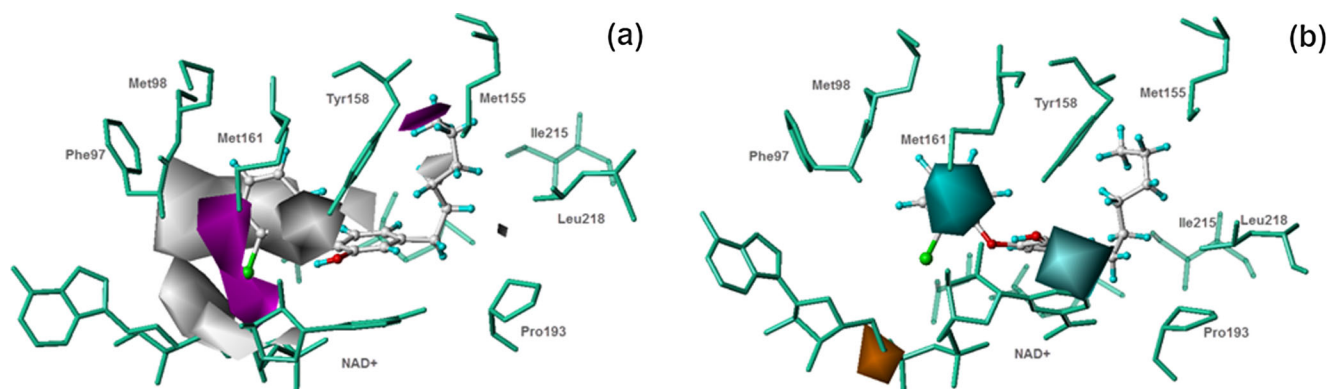

Fig. 7 CoMSIA hydrophobic (**a**) and hydrogen bond donor (**b**) contours in combination with compound **29** (ball and stick in atom type colors) in InhA binding pocket (stick in *greenblue*)

at the R_2, R_3 and R_4 substituents should be optimal for the InhA binding pocket. Moreover, the magenta and blue contours close to the R_2 substituent suggest additional structural requirement at this position, which should contain the hydrophobic property and less electron density. This suggestion is consistent with the MD results, which indicate that the R_2 position can be substituted with hydrophobic or hydrophilic groups so that the phenyl B ring could be favorable in binding with the methyl side chain of Ala198, and the pyrophosphate moiety of NAD^+, respectively. Apart from the hydrophobic properties, the R_2 substituent with the less electron density should be optimal for the pyrophosphate moiety of NAD^+ presenting the negative charge.

Conclusions

MD simulations were successfully applied to reliably predict binding modes, inhibitor–enzyme interactions, and binding free energies of diphenyl ether derivatives in the InhA binding pocket. The graphic interpretation of the obtained CoMSIA model reveals the key structural elements of diphenyl ether derivatives necessary for good InhA inhibitory activities. The structural requirements derived from the CoMSIA model correspond well with the binding interactions of diphenyl ether derivatives in the InhA pocket found in the MD simulations. The presented integrated results should be useful as guiding principles for the design of novel InhA inhibitors based on suitable modifications of the diphenyl ether scaffold.

References

1. World Health Organization (2013) Global tuberculosis report, Available at http://apps.who.int/iris/bitstream/10665/91355/1/9789241564656_eng.pdf

2. Quemard A, Sacchettini JC, Dessen A, Vilcheze C, Bittman R, Jacobs WR Jr, Blanchard JS (1995) Enzymatic characterization of the target for isoniazid in *Mycobacterium tuberculosis*. Biochemistry 34(36):8235–8241

3. Rozwarski DA, Vilchèze C, Sugantino M, Bittman R, Sacchettini JC (1999) Crystal structure of the Mycobacterium tuberculosis enoyl-ACP reductase, InhA, in complex with NAD^+ and a C16 fatty acyl substrate. J Biol Chem 274(22):15582–15589

4. Agüero F, Al-Lazikani B, Aslett M, Berriman M, Buckner FS, Campbell RK, Carmona S, Carruthers IM, Chan AW, Chen F, Crowther GJ, Doyle MA, Hertz-Fowler C, Hopkins AL, McAllister G, Nwaka S, Overington JP, Pain A, Paolini GV, Pieper U, Ralph SA, Riechers A, Roos DS, Sali A, Shanmugam D, Suzuki T, Van Voorhis WC, Verlinde CL (2008) Genomic-scale prioritization of drug targets: the TDR targets database. Nat Rev Drug Discov 7(11):900–907

5. Campbell JW, Cronan JE Jr (2001) Bacterial fatty acid biosynthesis: targets for antibacterial drug discovery. Annu Rev Microbiol 55:305–332

6. Heath RJ, Rock CO (2004) Fatty acid biosynthesis as a target for novel antibacterials. Curr Opin Invest Drugs 5(2):146–153

7. White SW, Zheng J, Zhang YM, Rock CO (2005) The structural biology of type II fatty acid biosynthesis. Annu Rev Biochem 74:791–831

8. Zhang YM, Lu YJ, Rock CO (2004) The reductase steps of the type II fatty acid synthase as antimicrobial targets. Lipids 39(11):1055–1060

9. Wen L, Chmielowski JN, Bohn KC, Huang JK, Timsina YN, Kodali P, Pathak AK (2009) Functional expression of *Francisella tularensis* FabH and FabI, potential antibacterial targets. Protein Exp Purif 65(1):83–91

10. Wright HT, Reynolds KA (2007) Antibacterial targets in fatty acid biosynthesis. Curr Opin Microbiol 10(5):447–453

11. Rozwarski DA, Grant GA, Barton DH, Jacobs WR Jr, Sacchettini JC (1998) Modification of the NADH of the isoniazid target (InhA) from *Mycobacterium tuberculosis*. Science 279(5347):98–102

12. Vilcheze C, Wang F, Arai M, Hazbon MH, Colangeli R, Kremer L, Weisbrod TR, Alland D, Sacchettini JC, Jacobs WR Jr (2006) Transfer of a point mutation in *Mycobacterium tuberculosis* InhA resolves the target of isoniazid. Nat Med 12(9):1027–1029

13. Dessen A, Quemard A, Blanchard JS, Jacobs WR Jr, Sacchettini JC (1995) Crystal structure and function of the isoniazid target of *Mycobacterium tuberculosis*. Science 267(5204):1638–1641

14. Johnsson K, Schultz PG (1994) Mechanistic studies of the oxidation of isoniazid by the catalase peroxidase from *Mycobacterium tuberculosis*. J Am Chem Soc 116(16):7425–7426

15. Lei B, Wei CJ, Tu SC (2000) Action mechanism of antitubercular isoniazid. Activation by *Mycobacterium tuberculosis* KatG, isolation, and characterization of InhA inhibitor. J Biol Chem 275(4):2520–2526

16. Johnsson K, King DS, Schultz PG (1995) Studies on the mechanism of action of isoniazid and ethionamide in the chemotherapy of tuberculosis. J Am Chem Soc 117(17):5009–5010

17. Zhang Y, Heym B, Allen B, Young D, Cole S (1992) The catalase-peroxidase gene and isoniazid resistance of *Mycobacterium tuberculosis*. Nature 358(6387):591–593

18. Banerjee A, Dubnau E, Quemard A, Balasubramanian V, Um KS, Wilson T, Collins D, de Lisle G, Jacobs WR Jr (1994) InhA, a gene encoding a target for isoniazid and ethionamide in *Mycobacterium tuberculosis*. Science 263(5144):227–230

19. Quemard A, Dessen A, Sugantino M, Jacobs WR Jr, Sacchetini JC, Blanchard JS (1996) Binding of catalase-peroxidase-activated isoniazid to wild-type and mutant *Mycobacterium tuberculosis* enoyl-ACP reductases. J Am Chem Soc 118(6):1561–1562

20. Saint-Joanis B, Souchon H, Wilming M, Johnsson K, Alzari PM, Cole ST (1999) Use of site-directed mutagenesis to probe the structure, function and isoniazid activation of the catalase/peroxidase, KatG, from *Mycobacterium tuberculosis*. Biochem J 338(Pt 3):753–760

21. Zhao X, Yu H, Yu S, Wang F, Sacchettini JC, Magliozzo RS (2006) Hydrogen peroxide-mediated isoniazid activation catalyzed by *Mycobacterium tuberculosis* catalase-peroxidase (KatG) and its S315T mutant. Biochemistry 45(13):4131–4140

22. Metcalfe C, Macdonald IK, Murphy EJ, Brown KA, Raven EL, Moody PC (2008) The tuberculosis prodrug isoniazid bound to activating peroxidases. J Biol Chem 283(10):6193–6200

23. Sinha BK (1983) Enzymatic activation of hydrazine derivatives. J Biol Chem 258(2):796–801

24. Nguyen M, Claparols C, Bernadou J, Meunier B (2001) A fast and efficient metal-mediated oxidation of isoniazid and identification of isoniazid-NAD(H) adducts. ChemBioChem 2(12):877–883

25. Heym B, Zhang Y, Poulet S, Young D, Cole ST (1993) Characterization of the katG gene encoding a catalase-peroxidase required for the isoniazid susceptibility of *Mycobacterium tuberculosis*. J Bacteriol 175(13):4255–4259

26. Timmins GS, Deretic V (2006) Mechanisms of action of isoniazid. Mol Microbiol 62(5):1220–1227

27. Johnsson K, Froland WA, Schultz PG (1997) Overexpression, purification, and characterization of the catalase-peroxidase KatG from *Mycobacterium tuberculosis*. J Biol Chem 272(5):2834–2840

28. De La Iglesia AI, Morbidoni HR (2006) Mechanisms of action of and resistance to rifampicin and isoniazid in *Mycobacterium tuberculosis*: new information on old friends. Rev Argent Microbiol 38(2):97–109

29. Parikh SL, Xiao G, Tonge PJ (2000) Inhibition of InhA, the enoyl reductase from *Mycobacterium tuberculosis*, by triclosan and isoniazid. Biochemistry 39(26):7645–7650

30. Freundlich JS, Wang F, Vilchèze C, Gulten G, Langley R, Schiehser GA, Jacobus DP, Jacobs WR Jr, Sacchettini JC (2009) Triclosan derivatives: towards potent inhibitors of drug-sensitive and drug-resistant *Mycobacterium tuberculosis*. ChemMedChem 4(2):241–248

31. am Ende CW, Knudson SE, Liu N, Childs J, Sullivan TJ, Boyne M, Xu H, Gegina Y, Knudson DL, Johnson F, Peloquin CA, Slayden RA, Tonge PJ, Ende CW, Knudson SE, Liu N, Childs J, Sullivan TJ, Boyne M, Xu H, Gegina Y, Knudson DL, Johnson F, Peloquin CA, Slayden RA, Tonge PJ (2008) Synthesis and in vitro antimycobacterial activity of B-ring modified diaryl ether InhA inhibitors. Bioorg Med Chem Lett 18(10):3029–3033

32. Boyne ME, Sullivan TJ, am Ende CW, Lu H, Gruppo V, Heaslip D, Amin AG, Chatterjee D, Lenaerts A, Tonge PJ, Slayden RA (2007) Targeting fatty acid biosynthesis for the development of novel chemotherapeutics against *Mycobacterium tuberculosis*: evaluation of A-ring-modified diphenyl ethers as high-affinity InhA inhibitors. Antimicrob Agents Chemother 51(10):3562–3567

33. Sullivan TJ, Truglio JJ, Boyne ME, Novichenok P, Zhang X, Stratton CF, Li HJ, Kaur T, Amin A, Johnson F, Slayden RA, Kisker C, Tonge PJ (2006) High affinity InhA inhibitors with activity against drug-resistant strains of *Mycobacterium tuberculosis*. ACS Chem Biol 1(1):43–53

34. Luckner SR, Liu N, am Ende CW, Tonge PJ, Kisker C (2010) A slow, tight-binding inhibitor of InhA, the enoyl-ACP reductase from *Mycobacterium tuberculosis*. J Biol Chem 285(19):14330–14337

35. Pan P (2012) Lead optimization and slow-onset inhibition of the enoyl-ACP reductase (InhA) from *Mycobacterium tuberculosis*. PhD Diss., Stony Brook University

36. Lu XY, Chen YD, Jiang YJ, You QD (2009) Discovery of potential new InhA direct inhibitors based on pharmacophore and 3D-QSAR analysis followed by in silico screening. Eur J Med Chem 44(9):3718–3730

37. Kumar A, Siddiqi MI (2008) CoMFA based de novo design of pyrrolidine carboxamides as inhibitors of enoyl acyl carrier protein reductase from *Mycobacterium tuberculosis*. J Mol Model 14(10):923–935

38. Andrade CH, Salum Lde B, Castilho MS, Pasqualoto KF, Ferreira EI, Andricopulo AD (2008) Fragment-based and classical quantitative structure-activity relationships for a series of hydrazides as antituberculosis agents. Mol Divers 12(1):47–59

39. Lu XU, Chen YD, You QD (2010) 3D-QSAR studies of arylcarboxamides with inhibitory activity on InhA using pharmacophore-based alignment. Chem Bio Drug Des 75(2):195–203

40. Punkvang A, Saparpakorn P, Hannongbua S, Wolschann P, Beyer A, Pungpo P (2010) Investigating the structural basis of arylamides to improve potency against *M. tuberculosis* strain through molecular dynamics simulations. Eur J Med Chem 45(12):5585–5593

41. Punkvang A, Saparpakorn P, Hannongbua S, Wolschann P, Pungpo P (2010) Elucidating drug-enzyme interactions and their structural basis for improving the affinity and potency of isoniazid and its derivatives based on computer modeling approaches. Molecules 15(4):2791–2813

42. Punkvang A, Saparpakorn P, Hannongbua S, Wolschann P, Berner H, Pungpo P (2010) Insight into crucial inhibitor–enzyme interaction of arylamides as novel direct inhibitors of the enoyl ACP reductase (InhA) from *Mycobacterium tuberculosis*: computer-aided molecular design. Monatsh Chem 141(9):1029–1041

43. Pauli I, dos Santos RN, Rostirolla DC, Martinelli LK, Ducati RG, Timmers LF, Basso LA, Santos DS, Guido RV, Andricopulo AD, Norberto de Souza O (2013) Discovery of new inhibitors of *Mycobacterium tuberculosis* InhA enzyme using virtual screening and a 3D-pharmacophore-based approach. J Chem Inf Model 53(9):2390–2401

44. Kinjo T, Koseki Y, Kobayashi M, Yamada A, Morita K, Yamaguchi K, Tsurusawa R, Gulten G, Komatsu H, Sakamoto H, Sacchettini JC, Kitamura M, Aoki S (2013) Identification of compounds with potential antibacterial activity against *Mycobacterium* through structure-based drug screening. J Chem Inf Model 53(5):1200–1212

45. Kumar UC, Bvs SK, Mahmood S, Sriram D, Kumar-Sahu P, Pulakanam S, Ballell L, Alvarez-Gomez D, Malik S, Jarp S (2013) Discovery of novel InhA reductase inhibitors: application of pharmacophore- and shape-based screening approach. Future Med Chem 5(3):249–259

46. Stigliani JL, Bernardes-Génisson V, Bernadou J, Pratviel G (2012) Cross-docking study on InhA inhibitors: a combination of Autodock Vina and PM6-DH2 simulations to retrieve bio-active conformations. Org Biomol Chem 10:6341–6349

47. Subba Rao G, Vijayakrishnan R, Kumar M (2008) Structure-based design of a novel class of potent inhibitors of InhA, the enoyl acyl carrier protein reductase from *Mycobacterium tuberculosis*: a computer modelling approach. Chem Biol Drug Des 72(5):444–449

48. Stigliani JL, Arnaud P, Delaine T, Bernardes-Génisson V, Meunier B, Bernadou J (2008) Binding of the tautomeric forms of isoniazid-NAD adducts to the active site of the *Mycobacterium tuberculosis* enoyl-ACP reductase (InhA): a theoretical approach. J Mol Graph Model 27(4):536–545

49. (2006) GaussView 03, Revision 3.07, Gaussian, Inc., Wallingford, CT

50. Frisch MJ, Trucks GW, Schlegel HB, Scuseria GE, Robb MA, Cheeseman JR, Scalmani G, Barone V, Mennucci B, Petersson GA, Nakatsuji H, Caricato M, Li X, Hratchian HP, Izmaylov AF, Bloino J, Zheng G, Sonnenberg JL, Hada M, Ehara M, Toyota K, Fukuda R, Hasegawa J, Ishida M, Nakajima T, Honda Y, Kitao O, Nakai H, Vreven T, Jr. JAM, Peralta JE, Ogliaro F, Bearpark M, Heyd JJ, Brothers E, Kudin KN, Staroverov VN, Kobayashi R, Normand J, Raghavachari K, Rendell A, Burant JC, Iyengar SS, Tomasi J, Cossi M, Rega N, Millam JM, Klene M, Knox JE, Cross JB, Bakken V, Adamo C, Jaramillo J, Gomperts R, Stratmann RE, Yazyev O, Austin AJ, Cammi R, Pomelli C, Ochterski JW, Martin RL, Morokuma K, Zakrzewski VG, Voth GA, Salvador P, Dannenberg JJ, Dapprich S, Daniels AD, Farkas O, Foresman JB, Ortiz JV, Cioslowski J, Fox DJ (2009) Gaussian 09, revision B.01, Gaussian Inc., Wallingford CT

51. Morris GM, Goodsell DS, Huey R, Olson AJ (1996) Distributed automated docking of flexible ligands to proteins: parallel applications of AutoDock 2.4. J Comput Aided Mol Des 10(4):293–304

52. Tripos International (2008) SYBYL v8.0, Tripos International, 1699 South Hanley Rd., St. Louis, MO

53. Golbraikh A, Tropsha A (2002) Beware of q^2! J Mol Graph Model 20:267–276

54. Case DA, Darden TA, Cheatham TE, Simmerling CL, Wang J, Duke RE, Luo R, Crowley M, Walker RC, Zhang W, Merz KM, Wang B, Hayik S, Roitberg A, Seabra G, Kolossvry I, Wong KF, Paesani F, Vanicek J, Wu X, Brozell SR, Steinbrecher T, Gohlke H, Yang L, Tan

C, Mongan J, Hornak V, Cui G, Mathews DH, Seetin MG, Sagui C, Babin V, Kollman PA (2008) AMBER12. University of California, San Francisco

55. Duan Y, Wu C, Chowdhury S, Lee MC, Xiong G, Zhang W, Yang R, Cieplak P, Luo R, Lee T, Caldwell J, Wang J, Kollman P (2003) A point-charge force field for molecular mechanics simulations of proteins based on condensed-phase quantum mechanical calculations. J Comput Chem 24(16):1999–2012

56. Wang J, Wang W, Kollman PA, Case DA (2006) Automatic atom type and bond type perception in molecular mechanical calculations. J Mol Graphics Model 25(2):247–260

57. Wang J, Wolf RM, Caldwell JW, Kollman PA, Case DA (2004) Development and testing of a general AMBER force field. J Comput Chem 25(9):1157–1174

58. Cornell WD, Cieplak P, Bayly CI, Kollman PA (1993) Application of RESP charges to calculation conformational energies, hydrogen bond energies, and free energies of salvation. J Am Chem Soc 115(21): 9620–9631

59. Bayly CI, Cieplak P, Cornell WD, Kollman PA (1993) A well-behaved electrostatic potential based method using charge-restraints for deriving charges: The RESP model. J Phys Chem 97(40):10269–10280

60. Wang J, Cieplak P, Kollman PA (2000) How well does a restrained electrostatic potential (RESP) model perform in calculating conformational energies of organic and biological molecules? J Comput Chem 21(12):1049–1074

61. Gavernet L, Gonzalez Funes JL, Blanch LB, Estiu G, Maresca A, Supuran CT (2010) Affinity of sulfamates and sulfamides to carbonic anhydrase II isoform: experimental and molecular modeling approaches. J Chem Inf Model 50(6):1113–1122

62. Li W, Fu J, Cheng F, Zheng M, Zhang J, Liu G, Tang Y (2012) Unbinding pathways of GW4064 from human farnesoid X receptor

as revealed by molecular dynamics simulations. J Chem Inf Model 52(11):3043–3052

63. Mahoney MW, Jorgensen WL (2000) A five-site model for liquid water and the reproduction of the density anomaly by rigid, nonpolarizable potential functions. J Chem Phys 112(20):8910–8922

64. Darden T, York D, Pedersen L (1993) Particle mesh Ewald: an N·log(N) method for Ewald sums in large systems. J Chem Phys 98(12):10089–10092

65. Ryckaert JP, Ciccotti G, Berendsen HJC (1977) Numerical integration of the Cartesian equations of motion of a system with constraints: molecular dynamics of n-alkanes. J Comp Phys 23(3):327–341

66. Homeyer N, Gohlke H (2012) Free energy calculations by the molecular mechanics Poisson–Boltzmann surface area method. Mol Inf 31(2):114–122

67. Wang J, Hou T, Xu X (2006) Recent advances in free energy calculations with a combination of molecular mechanics and continuum models. Curr Comput Aided Drug Des 2(3):95–103

68. Wang J, Morin P, Wang W, Kollman PA (2001) Use of MM-PBSA in reproducing the binding free energies to HIV1 RT of TIBO derivatives and predicting the binding mode to HIV1 RT of Efavirenz by docking and MM-PBSA. J Am Chem Soc 123(22):5221–5230

69. Hou T, Wang J, Li Y, Wang W (2011) Assessing the performance of the MM/PBSA and MM/GBSA Methods. 1. The accuracy of binding free energy calculations based on molecular dynamics simulations. J Chem Inf Model 51(1):69–82

70. Kaledin M, Brown A, Kaledin AL, Bowman JM (2004) Normal mode analysis using the driven molecular dynamics method. II. An application to biological macromolecules. J Chem Phys 121(12):5646–5653

71. Xue W, Qi J, Yang Y, Jin X, Liu H, Yao X (2012) Understanding the effect of drug-resistant mutations of HIV-1 intasome on raltegravir action through molecular modeling study. Mol BioSyst 8:2135–2144

72. Zar JH (1998) Biostatistical analysis. Prentice Hall, Upper Saddle River